Biomimetic fabrication of antibacterial calcium phosphates mediated by polydopamine

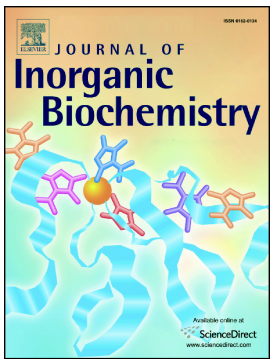

Biomimetic fabrication of antibacterial calcium phosphates mediated by polydopamine

Lucia Forte, Paola Torricelli, Francesca Bonvicini, Elisa Boanini, Giovanna Angela Gentilomi, Gigliola Lusvardi, Elena Della Bella, Milena Fini, Edoardo Vecchio Nepita, Adriana Bigi

PII: S0162-0134(17)30505-6
DOI: doi:10.1016/j.jinorgbio.2017.10.004
Reference: JIB 10349

To appear in: *Journal of Inorganic Biochemistry*

Received date: 11 July 2017
Revised date: 20 September 2017
Accepted date: 8 October 2017

Please cite this article as: Lucia Forte, Paola Torricelli, Francesca Bonvicini, Elisa Boanini, Giovanna Angela Gentilomi, Gigliola Lusvardi, Elena Della Bella, Milena Fini, Edoardo Vecchio Nepita, Adriana Bigi , Biomimetic fabrication of antibacterial calcium phosphates mediated by polydopamine. The address for the corresponding author was captured as affiliation for all authors. Please check if appropriate. Jib(2017), doi:10.1016/j.jinorgbio.2017.10.004

Biomimetic fabrication of antibacterial calcium phosphates mediated by polydopamine.

Lucia Forte[1], Paola Torricelli[2], Francesca Bonvicini[3], Elisa Boanini[1,*], Giovanna Angela Gentilomi[3], Gigliola Lusvardi[4], Elena Della Bella[2], Milena Fini[2], Edoardo Vecchio Nepita[5], Adriana Bigi[1]

[1] Department of Chemistry "Giacomo Ciamician", University of Bologna, via Selmi 2, 40126 Bologna, Italy

[2] Laboratory of Preclinical and Surgical Studies, Codivilla-Putti Research Institute, Rizzoli Orthopaedic Institute, via di Barbiano 1/10, 40136 Bologna, Italy

[3] Department of Pharmacy and Biotechnology, University of Bologna, via Massarenti 9, 40138 Bologna, Italy

[4]Department of Chemical and Geological Sciences, University of Modena and Reggio Emilia, via Campi 103, 41125 Modena, Italy

[5]Microbiology Operative Unit-Bacteriology Section, S. Orsola-Malpighi Hospital, via Massarenti 9, 40138 Bologna, Italy

* Corresponding author:

Elisa Boanini, PhD

Department of Chemistry “G. Ciamician”, University of Bologna

e-mail: elisa.boanini@unibo.it ; Tel: +39 051 2099548

Abstract

In this work we developed new antibacterial composite materials using polydopamine (PDA) to trigger the deposition of silver nanoparticles (AgNPs) onto calcium phosphates, namely octacalcium phosphate (OCP) and α-tricalcium phosphate (αTCP). Functionalization of OCP and αTCP with a self-polymerized polydopamine layer was obtained by soaking the calcium phosphates in dopamine solution. The PDA surface of functionalized calcium phosphates (OCPd and αTCPd) promoted the deposition of AgNPs by reducing silver ions when soaked in a silver nitrate solution. The amount of deposited AgNPs can be modulated by varying the concentration of silver nitrate solution and the type of substrate. The results of *in vitro* tests carried out with osteoblast-like MG63 cells indicate that the combination of AgNPs with OCP provides more biocompatible materials than those obtained using αTCP as substrate. In particular, the study of osteoblast activity and differentiation was focused on the samples OCPdAg5 (silver content = 8.2 wt%) and αTCPdAg5 (silver content = 4.7 wt%), which did not show any cytotoxicity, and compared with those obtained on pure OCP and αTCP. The results demonstrate that the AgNPs loaded materials support osteoblast viability and differentiation, whereas they significantly inhibit the growth of relevant antibiotic-resistant pathogenic bacteria.

Keywords: silver nanoparticles, octacalcium phosphate, α-tricalcium phosphate, polydopamine, multi-drug resistant bacteria, osteoblast

1. Introduction

Calcium phosphates (CaPs) are widely employed for the preparation of biomaterials for hard tissues substitution and repair, because of their similarity to the inorganic phase of the mineralized tissues of vertebrates. In particular, octacalcium phosphate, $Ca_8H_2(PO_4)_6 \bullet 5H_2O$ (OCP), which is considered the precursor phase of biological apatites, exhibits osteoconductive properties and converts into hydroxyapatite (HA) when implanted in bone defects [1]. Enhancement of bone formation has been demonstrated both when OCP granules are used to repair bone defects and when OCP is applied as a coating on metallic surfaces [2-6]. OCP can hydrolyze into HA in aqueous solution [7,8] However, the process is relatively slow at physiological pH and temperature, whereas it is accelerated at higher temperatures and in the presence of small amount of fluoride [9-12]. Also other CaPs, in particular α-tricalcium phosphate (αTCP), hydrolyze into HA [13]. At variance with OCP, αTCP is considered unsuitable for surgical implants [14]; however, it is widely employed for the preparation of calcium phosphate bone cements. αTCP has a relatively higher solubility than its polymorph, βTCP, and the hardening reaction of αTCP containing cements implies its conversion into HA [15,16]. One of the main problems of medical devices, including CaPs based biomaterials, is the relatively high risk of infections associated to their use. Silver nanoparticles (AgNPs) display antimicrobial properties against a broad spectrum of pathogens and are currently applied in a number of biomedical applications, including bone cements and implant coatings [17]. We have previously developed a fast and low cost procedure to support AgNPs on HA crystals, and shown that the composite material displays significant, long-standing antibacterial activity towards both *S. aureus* and *E. coli* [18]. In this study we propose to utilize OCP and αTCP, which are more soluble and resorbable than HA, as supports for AgNPs, using polydopamine (PDA) as

functionalizing and reducing agent. Polydopamine is a polymer formed under slightly basic conditions by the oxidative polymerization of dopamine, which creates a stable layer that is adherent to the surface of materials [19]. Stable PDA films with controlled thickness can be deposited on virtually any substrate. Moreover, PDA is biocompatible and exhibits several functional groups, such as catechol, amine and imine groups, which are able to react with a wide range of molecules [20]. In particular, the catechol group can oxidize into the corresponding quinone group and trigger reduction processes of metallic cations [21]. The peculiar characteristics of PDA prompted a number of studies that yielded an increasing number of new applications of PDA based materials, spanning in different fields, from energy to environment, to biomedical science [19]. Herein we optimized the experimental conditions to prepare PDA functionalized OCP and αTCP at increasing AgNPs contents, and we investigated the influence of the presence of AgNPs on the antibacterial properties of the composite materials against Gram positive and Gram negative reference bacterial strains, as well as against antibiotic-resistant clinical isolates recovered from patients with bone or prosthetic joint infections. Moreover, we tested the ability of the materials to support *in vitro* growth and differentiation of osteoblast-like cells MG63. MG63 activity and differentiation were investigated using the most common markers of osteoblast metabolism, which were tested both on the supernatants of cell culture and by means of quantitative polymerase chain reaction (qPCR).

2. Materials and Methods

2.1. Materials synthesis and characterization

The synthesis of OCP was carried out as previously reported [22]. Briefly, 250 ml of 0.04M $Ca(CH_3COO)_2 \bullet H_2O$ were added dropwise into 750 ml of a phosphate solution

containing 5 mmol of $Na_2HPO_4 \bullet 12H_2O$ and 5 mmol of $NaH_2PO_4 \bullet H_2O$ previously adjusted to pH 5 with CH_3COOH. The reaction was carried out at 60°C under mechanical stirring. After 15 min the precipitate was filtered, repeatedly washed with distilled water and dried at 37°C.

αTCP was obtained by solid-state reaction of a mixture of $CaCO_3$ and $CaHPO_4 \bullet 2H_2O$ in the molar ratio of 1:2 at 1300°C for 5 hours [23]. The solid product was carefully ground and sieved (<40 μm) before being submitted to further treatment.

Functionalization with polydopamine was obtained through immersion of 100 mg of OCP or αTCP into 50 ml of a solution of dopamine hydrochloride (2mg/ml) at pH 8.5 (TRIS buffer), under stirring [19], for different periods of time (1, 2 and 18 h) at room temperature. Then, the samples were filtered, repeatedly washed with distilled water and dried at 37°C overnight. In the following, the samples functionalized with PDA are indicated as OCPd and αTCPd, respectively.

Deposition of silver nanoparticles was obtained by simultaneous addition of 20 ml of $AgNO_3$ solution, at different concentrations (1, 5 and 10 mM), and 20 ml of a 13 mM sodium citrate solution, to the PDA functionalized phosphates (100 mg) at room temperature under stirring. After 1h, the solid samples were filtered, repeatedly washed with distilled water and dried at 37°C overnight. The two series of samples were labeled respectively OCPdAgX and αTCPdAgX, where X indicates the concentration (mM) of $AgNO_3$ solution.

X-ray diffraction analysis was carried out by means of a PANalytical X'Pert PRO powder diffractometer equipped with a X'Celerator detector (40 mA, 40 kV). For phase identification the 2θ range was investigated from 3 to 60 2θ degrees with a step size of 0.1 and time/step of 100 s.

Thermogravimetric analysis was carried out using a Perkin- Elmer TGA-7. Heating was performed in a platinum crucible in air flow (20 cm^3/min) at a rate of 10°C/min up to

700°C. The samples weights were in the range 5–10 mg. Results from this analysis represent the mean value of determinations for three different samples of each composition.

Morphological investigations of crystals were performed using a Phenom ProX desktop-scanning electron microscope at beam acceleration voltage of 10 kV. The samples were observed as prepared and not sputter coated before examination.

The quantification of Ag was performed using a quadrupole mass spectrometer with plasma source ICP MS XSeries Thermo Fisher Scientific. The samples were prepared by dissolving 10 mg of powders in water/ methanol solution 1/1 V/V. 5 ml were taken and added in 50 ml of 5% nitric acid solution.

Static contact angle measurements were performed on disk shaped samples (Ø = 13.0 mm). Each disk was prepared by pressing 100 mg of powder into cylindrical moulds by using a standard evacuable pellet die (Hellma). A KSV CAM101 instrument was used under ambient conditions by recording the side profiles of deionized water drops for image analysis. The shape of the drop was recorded in a time range of 0–60 s, by collecting an image every 0.033 s. At least six drops were observed for each sample.

In vitro and antibacterial tests were performed on disk-shaped samples (Ø= 6.0 mm). Each disk was prepared by pressing 40 mg of powder into cylindrical moulds by using a standard evacuable pellet die (Hellma), and sterilized using gamma rays (Cobalt-60) at a dose of 25 kGy.

AFM analysis of the disk-shaped samples was performed using a Veeco Nanoscope 3D instrument. The samples were analyzed in tapping mode using an E scanner (maximum scan size 15 μm) and phosphorus (n) doped silicon probes (spring constant 20–80 N/m; resonance frequency 250–290 kHz; nominal tip radius <10 nm). Roughness parameters, namely arithmetic mean roughness (Ra), root-square roughness (Rq), and the vertical

distance between the highest and lowest points within the evaluation length (Rt), were recorded.

Silver release was measured in the medium used for cell culture differentiation (see section 2.2.2.). The surnatants were removed from the wells at 1, 2 and 7 days and Ag content was analyzed using a quadrupole mass spectrometer with plasma source ICP MS XSeries Thermo Fisher Scientific.

2.2. Cellular tests

2.2.1. Cytotoxicity tests

Human osteoblast-like cells MG63 (OB, Istituto Zooprofilattico Sperimentale IZSBS, Brescia, Italy), were cultured in DMEM medium (Dulbecco's Modified Eagle's Medium, Sigma, UK) supplemented with 10% FCS, and antibiotics (100 U/ml penicillin, 100 μg/ml streptomycin). Cells were detached from culture flasks by trypsinization, and cell number and viability were checked by Erythosine B dye exclusion test. OB cells were plated at a density of $5x10^4$ cells/ml in 24-well plates containing sterile disk-shaped samples (Ø= 6.0 mm) (of the following biomaterial: OCPdAg1, OCPdAg5, OCPdAg10, αTCPdAg1, αTCPdAg5, αTCPdAg10. Wells for negative (CTR–, DMEM only) and positive (CTR+, DMEM + 0.05% phenol solution) controls were also prepared. Plates were cultured in standard conditions, at 37 ± 0.5°C with 95% humidity and 5% ± 0.2 CO_2 up to 72 hours.

The quantitative evaluation of cytotoxicity was performed by measuring cell viability, lactate dehydrogenase enzyme (LDH) release, Interleukin-6 (IL-6) and Caspase 3 activity. Cell proliferation and viability at 24 and 72 hours was assessed by WST1 (WST1, Roche Diagnostics GmbH, Manheim, Germany) colorimetric reagent test. The assay is based on the reduction of tetrazolium salt into a soluble formazan salt by a reductase of the mitochondrial respiratory chain, active only in viable cells. 100 μl of

WST1 solution and 900 µl of medium (final dilution: 1:10) were added to the cell monolayer, and the multi-well plates were incubated at 37°C for a further 4 h. Supernatants were quantified spectrophotometrically at 450 nm with a reference wavelength of 625 nm. Results of WST1 are reported as optical density (OD) and directly correlate with the cell number. Proliferation percent relative to CTR− are also reported. At the end of experimental times the supernatant was collected from all wells and centrifuged to remove particulates, if any, for LDH measure (LDH enzyme-kinetic test, Roche, D) and IL-6 (ELISA kit. Boster Biological Technology, Ca, USA) according to manufacture instruction. Cell lysate from all groups were collected at 72 h for the detection of Caspase 3 activity by an immunoenzymatic test (Caspase-e ELISA kit, Invitrogen, CA, USA).

A qualitative analysis for cell morphology was performed by Neutral Red (NR) vital staining. A 0.033% solution of NR staining (Sigma, UK) in culture medium was added to each group samples at the end of experimental time, for further 90 min. Cultures were examined by optical microscopy for the evaluation of cell morphology.

2.2.2. Bioactivity tests

OB were expanded in DMEM supplemented with 10% FCS, 1% antibiotics (100 U/ml penicillin, 100 µg/ml streptomycin), β-Glicerophosphate (10^{-4}M) and Ascorbic acid (50 µg/ml), counted and plated on material samples (OCP, OCPdAg5, αTCP, αTCPdAg5) at a concentration of $2x10^4$ cells/well in 24 wells-plates. OB were also seeded in empty wells for control (CTR). Plates were incubated at 37°C in a humidified 95%air/5%CO_2 atmosphere (standard condition) up to 7 days. Medium was changed with fresh medium to all wells after 3 days of culture.

Cell viability. At 7 days cell viability was observed by the Live/Dead® assay (Molecular Probes, Eugene, OR, USA), according to the manufacturer's instructions. Samples were visualized using an inverted microscope equipped with an

epifluorescence setup (Eclipse TiU, NIKON Europe BV, NITAL SpA, Milan, Italy): excitation/emission setting of 488/530 nm to detect green fluorescence (live cells) and 530/580 nm to detect red fluorescence (dead cells).

OB proliferation and viability was quantitatively evaluated by WST1 at the end of experimental time according to the method described above.

Osteoblast activity. At the end of experimental time, after 7 days of culture, the supernatant and cell lysate were collected from all wells. Aliquots were dispensed in Eppendorf tubes for storage at -70°C and assayed with the following immunoenzymatic kits: Alkaline Phosphatase (ALP, Cloud-Clone Corp, Wuhan, China), and Osteocalcin (OSTC, Cloud-Clone Corp), Caspase 3 (Life Technologies, Frederick, MD, USA). All results were normalized by CTR group.

Osteoblast morphology. At the end of experimental time, osteoblasts were fixed (2.5% glutaraldehyde in PBS pH 7.4 for 1 h), dehydrated in a graded ethanol series, and then treated with hexamethyldisilazane. SEM images were collected using a Hitachi S-2400 instrument operating at 15 kV on Pd coated samples.

Quantitative Polymerase Chain Reaction (qPCR). Total RNA was extracted from all samples at the end of experimental time using PureLink RNA Mini Kit (Life Technologies, Carlsbad, CA, USA). Purified RNA was reverse transcribed with Superscript VILO cDNA Synthesis kit (Invitrogen, Life Technologies, Carlsbad, CA, USA), following manufacturer's instructions. Each sample (10 ng) was tested in duplicate. qPCR analysis was performed in a LightCycler Instrument (Roche Diagnostics GmbH, Mannheim, Germany) using the QuantiTect SYBR Green PCR kit (Qiagen, Hilden, Germany). The protocol included a denaturation at 95°C for 15', 40 cycles of amplification (95°C 15'', appropriate annealing temperature for each target as detailed in Table S1 for 20'' and 72°C for 20'') and a melting curve to check for amplicon specificity. The threshold cycle (Ct) was determined for each sample. Relative

gene expression was calculated with the $2^{-\Delta\Delta Ct}$ method, using the control samples as calibrator.

2.2.3. Statistical Analysis

Statistical evaluation of data was performed using the software package SPSS/PC^{+} Statistics ^{TM} 23.0 (SPSS Inc., Chicago, IL USA). The results presented are the mean of six independent values. Data are reported as mean ± standard deviations (SD) at a significance level of $p<0.05$. After having verified normal distribution and homogeneity of variance, a one-way ANOVA was done for comparison between groups. Finally, a post hoc multiple comparison tests was performed to detect significant differences among groups, and Pearson test was performed to detect correlation between data.

2.3 Bacterial strains and antibacterial susceptibility testing

The *in vitro* antibacterial activity of the OCPd and αTCPd samples loaded with different amounts of Ag was evaluated against a panel of Gram positive and Gram negative reference bacterial strains including *Staphylococcus aureus* (ATCC 25923), *Staphylococcus epidermidis* (ATCC 12228), *Enterococcus faecalis* (ATCC 29212), *Escherichia coli* (ATCC 25922), *Klebsiella pneumoniae* (ATCC 9591) and *Pseudomonas aeruginosa* (ATCC 27853). Subsequently, having defined both the overall spectrum of antibacterial activity and the cytotoxic profile of the tested samples, the OCPdAg5 and αTCPdAg5 materials were assayed towards 14 clinical isolates recovered from patients with bone or prosthetic joint infections (7 *S. epidermidis* and 7 *P. aeruginosa* strains). Clinical strains were isolated on BD Columbia Agar with 5% sheep blood (Becton Dickinson, GmbH, Germany) and confirmed by MALDI-TOF MS analysis (Bruker Daltonics, GmbH, Germany) [24]. Their antibiotic susceptibility was determined by using the Vitek2 semi-automated system (bioMerieux, France); EUCAST criteria were used for the interpretation of results and categorization of strains

(Sensitive, Intermediate or Resistant strains) (www.eucast.org). Isolates resistant to ≥ 3 antibiotic groups tested were considered multi-drug resistant (MDR).

The effectiveness of the composite materials to inhibit bacterial growth was determined by means of standardized sensitivity tests based on Kirby-Bauer (KB) diffusion method and following the procedures established by a number of committees [25,26]. Briefly, the surface of Mueller-Hinton agar plate (MHA) (Sigma-Aldrich) was inoculated with the bacterial suspension at 0.5 McFarland, prepared in sterile 0.9% saline solution and gamma rays sterilized disks (Ø = 6.0 mm) were placed on the agar plates. In compliance with the International guidance documents in susceptibility testing, disks containing gentamicin (GMN 10 μg) and/or imipenem (IPM 10 μg) (Oxoid SpA, Italy) were included as reference controls. After 24 hours of incubation at 37°C the agar plate was observed and the diameter of the inhibition zone (corresponding to the bacterial-free zone around the disk-shaped sample) was measured and expressed in millimeters (mm). All experiments were performed on duplicate in different days.

3. Results and discussion

3.1 Materials characterization

The amount of PDA deposited on OCP and αTCP can be evaluated through thermogravimetric analysis. In fact, PDA undergoes thermal decomposition between about 250 and 650 °C, and its relative content can be determined as difference between the total weight loss of functionalized samples and that of the pristine calcium phosphates (Figure S1). The data reported in Table 1 indicate that the amount of deposited PDA increases with immersion time, in agreement with previous studies [19]. However, the amount of PDA deposited onto αTCP is always significantly higher than onto OCP, most likely because of the different morphology of the two calcium

phosphates. In fact, SEM images of OCP and αTCP immersed in dopamine solution for different periods of time (Figure S2) confirm the greater amount of the polymer deposited onto αTCP porous particles than onto OCP flat crystals.

Table 1 - Polydopamine content (determined through thermogravimetric analysis) of the different samples as a function of time. The values of contact angles and water absorption time are also reported.

Substrate	Time (h)	PDA content (wt %)	Static Contact Angle θ (°)	Absorption time (sec)
OCP	-	-	28 ± 1	2
OCPd	1	<1	43 ± 2	11
OCPd	2	2.1 ± 0.5	45 ± 2	>15
OCPd	18	10.4 ± 1.0	65 ± 3	>>15
αTCP	-	-	23 ± 2	1
αTCPd	1	2.4 ± 0.5	32 ± 1	1
αTCPd	2	6.5 ± 0.7	53 ± 2	3
αTCPd	18	25.7 ± 2.2	55 ± 2	12

However, PDA onto αTCP appears clustered into aggregates whereas it seems more spread in close contact with the large surface of OCP crystals. Moreover, the samples obtained after immersion for 18 hours show a massive dopamine polymerization that occurs without a close relationship with the calcium phosphates. On this basis, deposition of AgNPs was carried out on PDA functionalized samples obtained using an immersion time of 2 hours.

The deposition of PDA provokes also variations in the values of contact angle and time required for water complete spreading on the surface, which increase with PDA content (Table1). This finding is somewhat opposite to what usually verified in other studies where PDA deposition induces a decrease of the contact angle with respect to that of the support [27,28]. However, at variance with the supports used in those studies, both OCP and αTCP are highly hydrophilic, in agreement with their low contact angles and water

spreading times (Table 1). The modest increase of the values of these parameters on increasing PDA could be ascribed to the less homogeneous surfaces of the composite samples due to the presence of the polymer.

The XRD patterns of the functionalized calcium phosphates after AgNPs deposition show the characteristic reflections of OCP (PDF 26-1056) and αTCP (PDF 9-348) respectively, together with a reflection at about 38.1° of 2θ corresponding to the most intense peak of silver (PDF 4-783) (Figure 1). The relative intensity of this reflection increases with the concentration of the $AgNO_3$ solution used for the deposition.

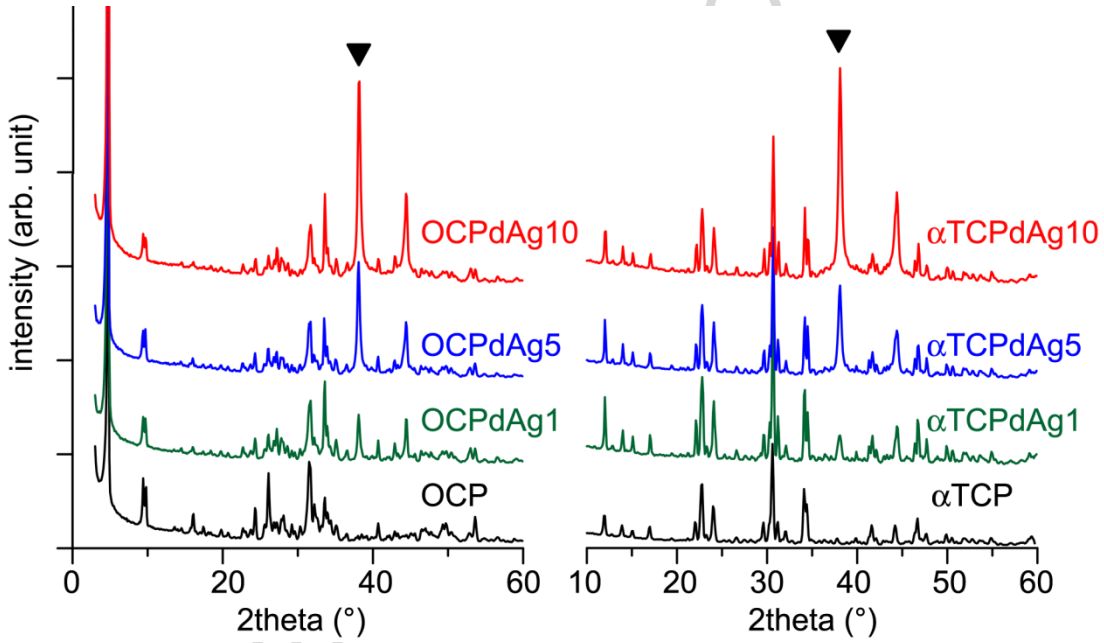

Figure 1 - XRD patterns of the different samples. The main diffraction peak due to Ag is indicated with (▼). The relative intensity of this reflection increases on increasing the concentration of the silver nitrate solution.

The presence of AgNPs onto the surface of OCPd and αTCPd is appreciable also in the SEM images of the composite materials. In particular, AgNPs appear more homogeneously distributed on the OCPd crystals surfaces than on αTCPd particles (Figure 2).

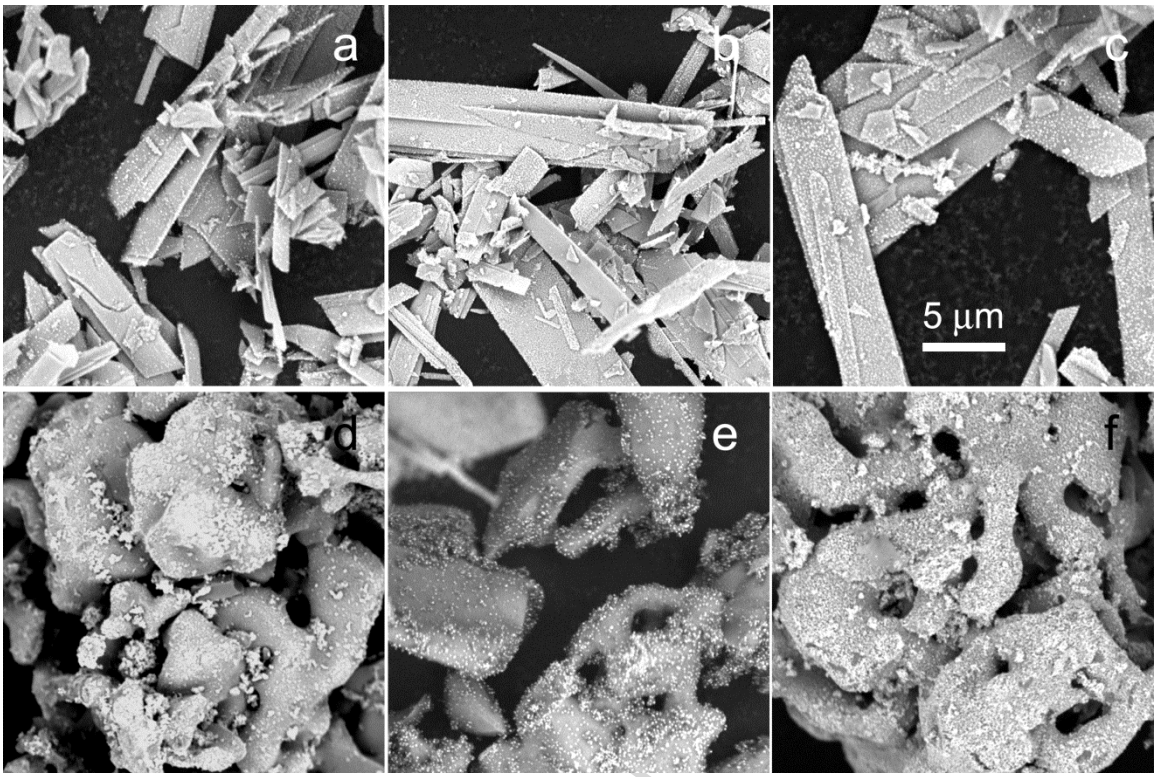

Figure 2 - SEM images of (a) OCPdAg1, (b) OCPdAg5, (c) OCPdAg10, (d) αTCPdAg1, (e) αTCPdAg5, (f) αTCPdAg10.

The results of ICP investigation reported in Table 2 indicate that the amount of AgNPs associated to OCPd and αTCPd increases with silver concentration in solution up to about 11.6 and 6.8 wt%, respectively. The greater deposition of AgNPs onto OCPd cannot be ascribed to a greater presence of PDA, since its content (2.1%) its smaller than on αTCPd (6.5%), and it might be due to the morphology of the big plate-like crystals of octacalcium phosphate, which favors a more homogeneous deposition of PDA, and, as a consequence, of AgNPs.

Table 2 - Ag content (wt%) determined through ICP analysis of solid samples obtained after immersion of OCPd and αTCPd into solutions at different concentration of $AgNO_3$

Samples	OCPdAg1	OCPdAg5	OCPdAg10	αTCPdAg1	αTCPdAg5	αTCPdAg10
Ag content (wt %)	1.6 ± 0.1	8.2 ± 0.2	11.6 ± 0.2	0.8 ± 0.1	4.7 ± 0.1	6.8 ± 0.2

3.2 In vitro tests

In vitro osteoblast cytotoxicity, viability and differentiation, as well as antibacterial tests were performed on disk-shaped samples, which were prepared by pressing the sample powders, as reported in Materials and Methods. The different morphology of OCP and αTCP are still appreciable on the surfaces of the disks, as results from the AFM images reported in Figure 3. The mean values of roughness parameters are Rq = 43 ± 4 nm, Ra = 30 ± 4 nm, Rt = 390 ± 41 nm for OCP, and Rq = 75 ± 8 nm; Ra = 55 ± 6 nm; Rt = 600 ± 63 nm for αTCP. No appreciable difference in the roughness parameters has been determined after AgNPs deposition on both substrates, although the surface morphology appears less defined (Figure 3) most likely because of the presence of PDA, which gives a different interaction with the AFM probe in comparison with the harder inorganic phases.

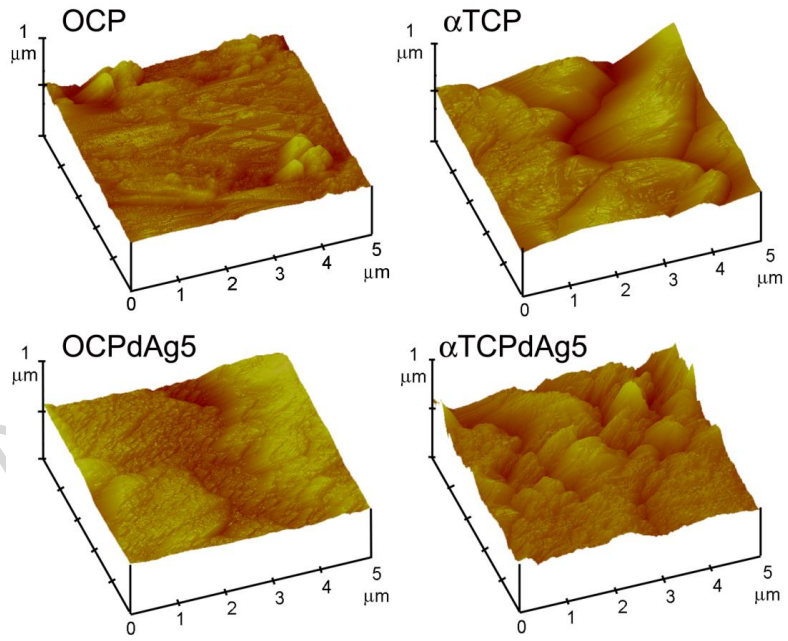

Figure 3 - AFM images of the surface of disk-shaped samples used for *in-vitro* tests.

Silver release from OCPdAg5 and αTCPdAg5 during *in vitro* cell tests was measured in cell culture medium. The cumulative release from OCPdAg5 and αTCPdAg5 increases with time and reaches values of 3.7 µg/ml and 5.2 µg/ml respectively after 7 days, as shown in Figure 4. The amount of silver release is greater from αTCPdAg5 than from OCPdAg5, most likely due to their different roughness, but it is however very small, < 1 wt% of the initial content.

The structure and morphology of the disk shaped samples after 7 days immersion in cell medium are compared with those of the starting samples in Figures S3 and S4. XRD patterns of OCPdAg5 and αTCPdAg5 do not show any appreciable modifications after incubation. However, at variance with OCPdAg5, which does not show any appreciable morphological change, the SEM image of the surface of αTCPdAg5 after immersion displays the presence of small crystals, most likely due to deposition from the supersaturated medium. It is conceivable to suppose that the amount of deposition is under the detection limit of XRD technique.

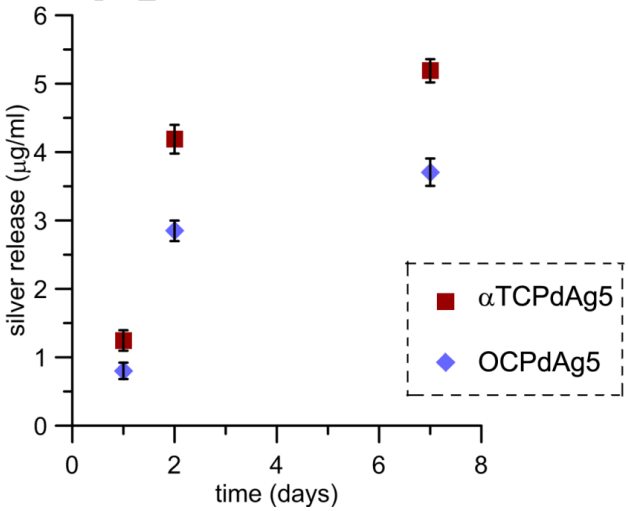

Figure 4 - Silver ions release from disk-shaped samples of OCPdAg5 and αTCPdAg5 after incubation in the medium used for cell culture differentiation up to 7 days.

3.2.1. Cell cytotoxicity.

MG63 are an osteoblast cell line well characterized and widely used in *in vitro* studies. Even if they display some differences in comparison to primary osteoblast in morphology and proliferation rate, they express the main markers of osteoblast differentiation useful for in vitro studies, have the advantage of a standard behaviour and are chosen to assess biomaterial biocompatibility.

At the end of experimental times, scheduled tests were performed to analyze cytotoxicity after OB culture with samples of OCP and αTCP at different AgNPs content. The percentage of viability in comparison to CTR- (considered as 100%) reported in Figure 5 shows that all samples values are lower than CTR-, both at 24 and 72 hours of culture ($p<0.0005$). Nevertheless, as a material is considered cytotoxic when its viability is less than 70% in comparison to CTR-, only samples OCPdAg10 and αTCPdAg10 may be considered cytotoxic [29]. As expected, CTR+ was significant lower than all experimental samples and CTR-. Further analysis of possible cytotoxic effects was performed through evaluation of LDH, Caspase 3 and IL-6. LDH is an intracellular enzyme and its detection in the supernatant of cell culture is considered a sign of cytotoxicity as a consequence of cytoplasmatic membrane damage [29]. At 24 h significant LDH level was detected only in αTCPdAg10 when compared to CTR-. At 72 h OCPdAg10 and all AgNPs containing αTCP groups were significantly higher than CTR-. CTR+ was significantly different from all groups both at 24 and 72 h.

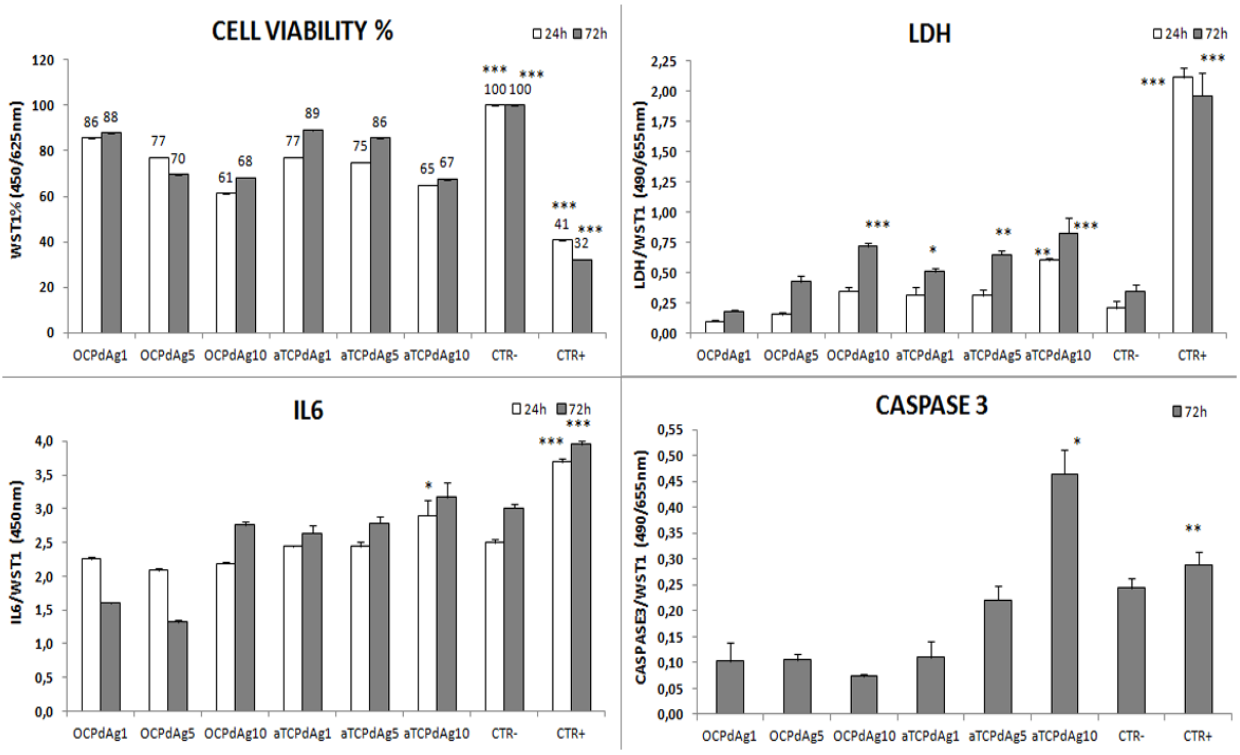

Figure 5 - Viability and cytotoxicity tested on OB grown on OCP or αTCP with different concentration of Ag, after 24 or 72 hours of culture. Statistical significance: (*p<0,05; **p<0,005; ***p<0,0005):

WST1: ***CTR+ and CTR- vs all experimental samples

LDH: ***CTR+ vs all at both 24 and 72 h; ***OCPAg10 and αTCPdAg10 vs CTR- (72h); **αTCPdAg5 vs CTR- (72h); **αTCPdAg10 vs CTR- (24h); *αTCPdAg1 vs CTR- (72h)

IL-6: ***CTR+ vs all at both 24 and 72 h; *αTCPdAg10 vs CTR- (24h)

CASPASE 3: **CTR+ vs all; *αTCPdAg10 vs CTR-

Apoptosis mechanism, expressed through extrinsic and intrinsic pathways, involves the activation of Caspase 3 through a cascade reaction. This protease activity has an essential role in protein degradation and cell death [30]. Moreover, OB in response to a cytotoxic agent produce different soluble inflammatory mediators as IL-6, that plays an important role in local regulation of bone turnover [31]. Caspase 3 (72h) and IL-6 (24h) were significantly higher than CTR- only in αTCPdAg10.

It is worthwhile to notice that AgNPs content of αTCPdAg10 is lower than that of OCPdAg5 and OCPdAg10, as shown in Table 2. It follows that the above reported results suggest that the combination of AgNPs with OCP provides more biocompatible materials than those obtained using αTCP as substrate.

Representative pictures of cultured cells at 24 hours after Neutral Red staining are showed in Figure 6. All samples show a significant uptake of dye, even if they display different cell concentration, In particular, the cells on OCPdAg10 and αTCPdAg10 display irregular shape, at variance with the other samples, which exhibit normal cell morphology.

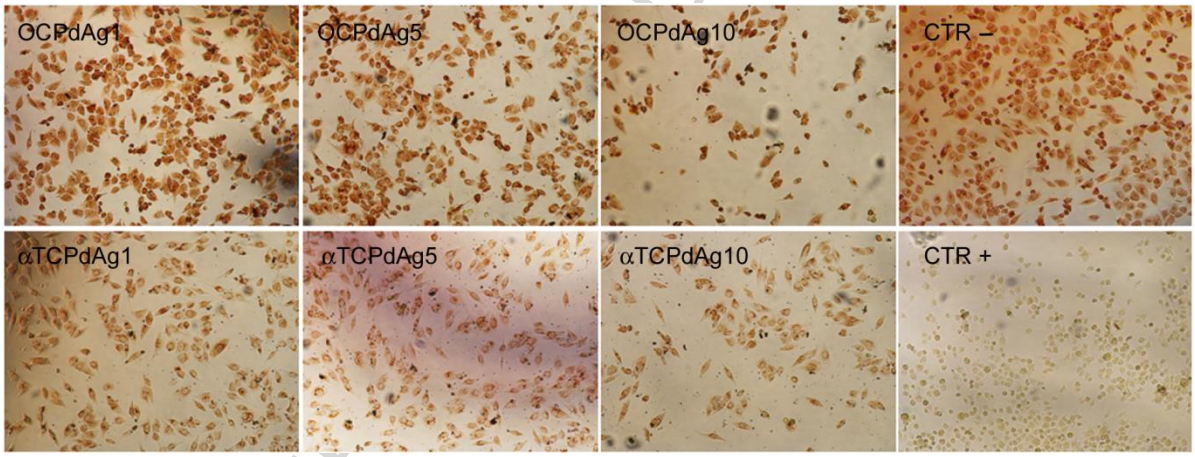

Figure 6 - Neutral Red staining of OB cultured for 72h on OCP, αTCP and CTRs. Living cells actively incorporated red dye, and grow adhering to the substrate showing a normal morphology. Dead cells, as CTR+ image, did not uptake dye, appeared round and detached from the substrate surface.

3.2.2. Cell bioactivity

On the basis of the results of the cytotoxicity tests, further investigation on biocompatibility and bioactivity was performed on OCPdAg5 and αTCPdAg5, as well as on OCP and αTCP. Both OCP and αTCP are known to be effective in improving osteoblast activity [32-37]. The results of cytotoxicity tests indicate that the presence of AgNPs in OCPdAg5 and αTCPdAg5 should not interfere with cellular activity, while exerting its local action to prevent bacterial infections [38].

Osteoblast viability. The evaluation of cell proliferation and viability was performed after 7 days of culture, by Live/Dead staining and WST1 test (Figure 7 and 8 respectively). Even if a higher number of cells was observed onto OCP in comparison to αTCP, pictures of osteoblasts demonstrated that cells cultured onto biomaterials, with or without Ag, grew and proliferated regularly, showing a normal morphology, as confirmed by SEM images, which show cells well spread and rich of philopodia. Differences on cell number are appreciable, in agreement with viability and proliferation test (Figure S5). Cell adhered to the different substrates and their adhesion was not affected by the presence of AgNPs (Figure 7).

These results were confirmed by the analysis of WST1 test: results showed significant higher values for OCP and OCPdAg5 when compared to both αTCP and αTCPdAg5 (figure 8), confirming the different influence of OCP and αTCP on viability. The viability percentage at 7 days of all groups (OCP 120%, OCPAg5 111%, αTCP 73%, αTCPAg5 78%) resulted higher than 70% in comparison with CTR group (considered as 100%), demonstrating absence of cytotoxicity [29]. Moreover no differences in viability where found between OCP and OCPdAg5, and between αTCP and αTCPdAg5.

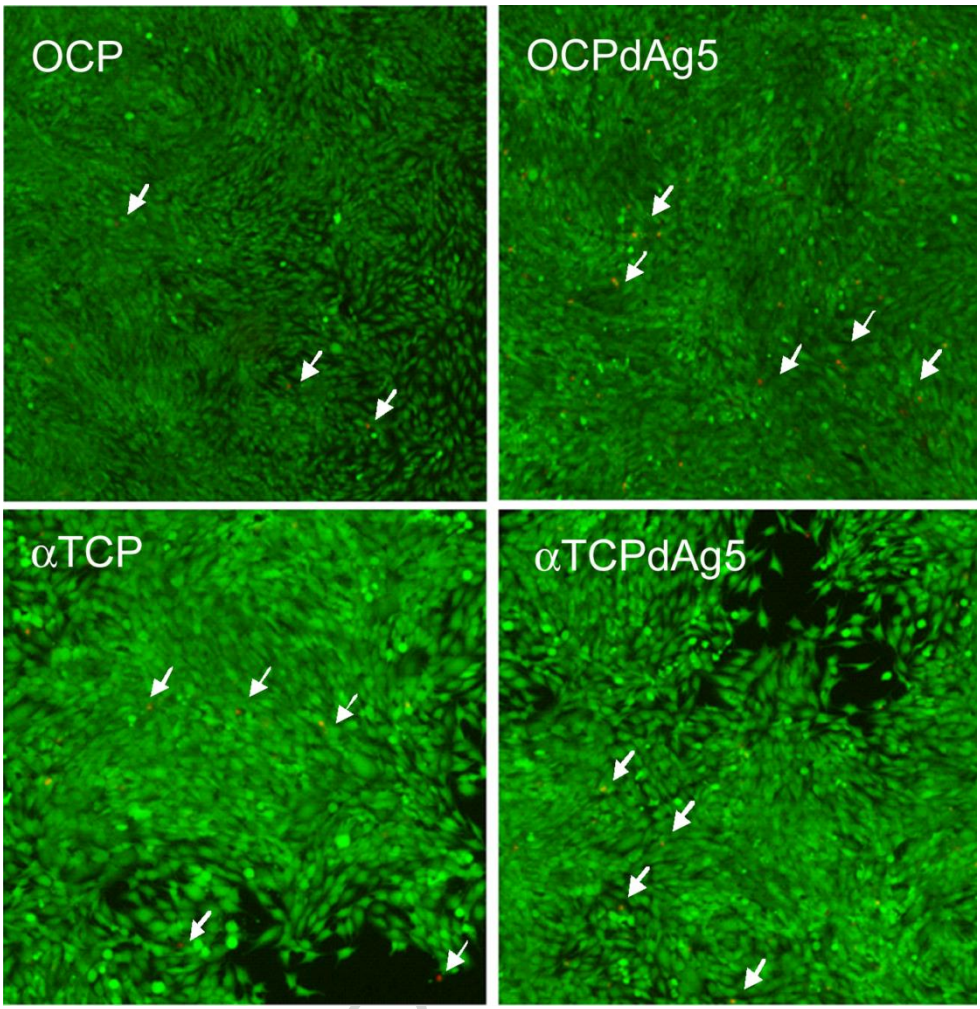

Figure 7 - Live/Dead staining of osteoblast cultured for 7 days on OCP, OCPdAg5, αTCP, and αTCPdAg5. Cells proliferated regularly onto the surface of all samples and adhered to the surface of biomaterials, showing normal morphology. Arrows point out dead red cells.

Osteoblast activity and gene expression. To complete the assessment of the effects of the studied biomaterials on osteoblasts, the activated Caspase 3, as a key role molecule in the main pathway of apoptosis [30], was measured. The production of ALP and OSTC was also measured at 7 days, as they represent common markers of the activity of differentiated osteoblasts [38]. After 7 days of culture no difference was found for Caspase 3 neither between materials with or without AgNPs, nor between materials and CTR (considered equal to 1) (Figure 8). Statistical analysis found that Caspase 3 values

were inversely correlated with WST1 data ($p<0.005$), and in agreement with Live/Dead staining. In fact, as a very low number of red dead cells was observed in all samples (indicated by arrows in Figure 7), the lower number of cells on αTCP samples may be related to a lower rate of proliferation rather than to cell death for apoptosis. Both ALP and OSTC data after 7 days of culture showed significant differences in comparison with CTR (normalized to 1, $p<0.05$), but no differences were found among materials (Figure 8). Results of ALP activity and OSTC production demonstrated that both OCP and αTCP stimulated osteoblast activity and differentiation, and that the presence of AgNPs did not interfere with culture.

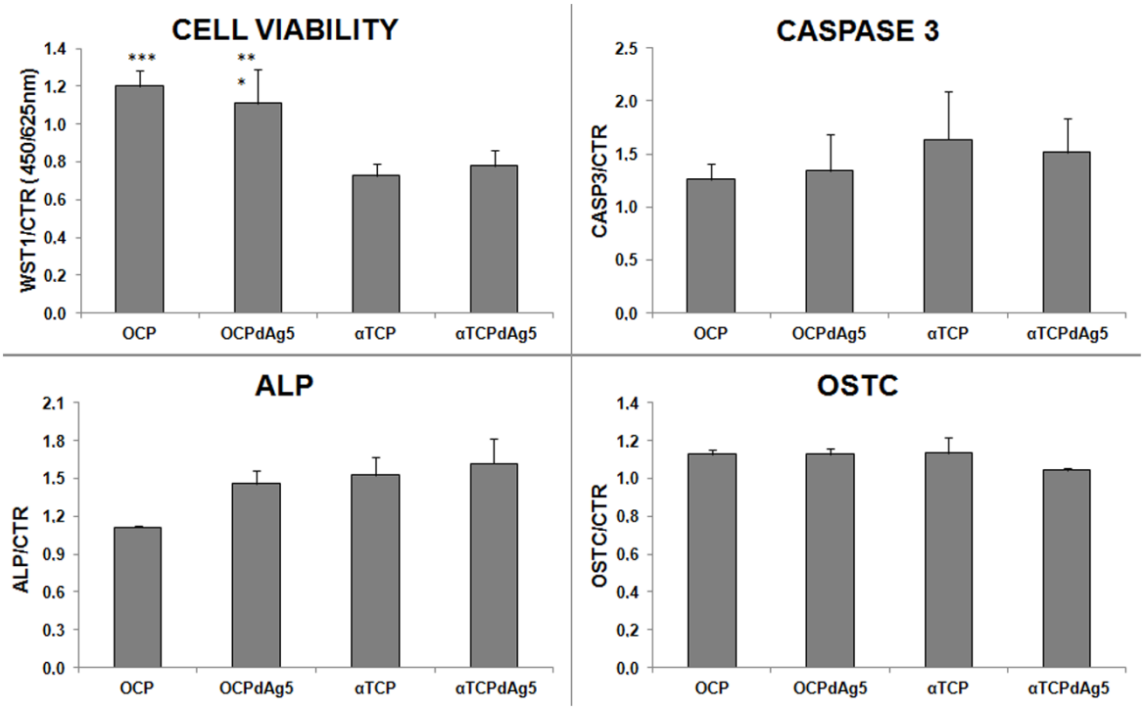

Figure 8 - Osteoblast viability and activity after 7 days of culture on OCP, OCPdAg5, αTCP, and αTCPdAg5. (*p<0,05; **p<0,005; ***p<0,0005)

WST1. ***OCP vs αTCP, αTCPdAg5; **OCPdAg5 vs αTCP; *OCPdAg5 vs αTCPdAg5

The measure of gene expression for the proteins detected in supernatant by immune-enzymatic assays, namely *CASP3*, *ALPL*, and *BGLAP* (OSTC), was also performed at the end of experimental time (Figure 9). Moreover *RUNX2* gene was investigated to verify if osteoblast maintained their differentiation [39]. The results, compared to CTR, demonstrated that gene expression did not differ from CTR and that there were no differences among biomaterials for *CASP3*, *ALPL*, and *RUNX2*. Although no differences were found for OSTC production detected in culture supernatant, *BGLAP* expression in OB cultured onto OCP at the same time point showed a significant higher level in comparison with αTCP and αTCPdAg5. To conclude the analysis of data, *ALPL*, *BGLAP* and *RUNX2* were found to directly correlate ($p<0.005$), as a confirmation of data consistency.

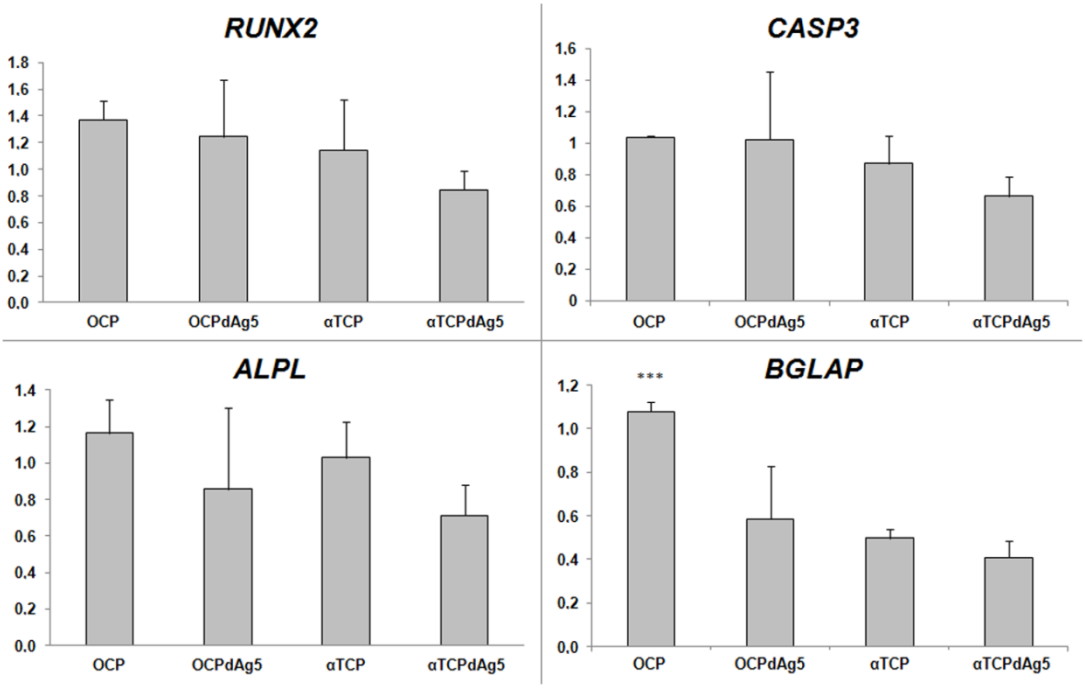

Figure 9 - Gene expression of osteoblast cultured for 7 days on OCP, OCPdAg5, αTCP, and αTCPdAg5. (*p<0,05; **p<0,005; ***p<0,0005)

BGLAP. ***OCP vs αTCP, αTCPdAg5 p<0,0005

3.3 Antibacterial susceptibility testing against bacterial strains

In a preliminary set of experiments, the *in vitro* antibacterial activity of OCPd and αTCPd samples loaded with different contents of AgNPs was determined against three Gram positive (*S. aureus*, *S. epidermidis*, *E. faecalis*) and three Gram negative (*E. coli*, *K. pneumoniae* and *P. aeruginosa*) reference strains. Results demonstrated that all composite materials, regardless their AgNPs content, inhibited bacterial growth as a clear bacterial-free zone was observed around the disks following a 24h-incubation. In particular, among Gram positive bacteria, the highest inhibitory activity was displayed against *S. epidermidis* while the effectiveness of the compounds was remarkable towards all the Gram negative bacteria and did not differ among tested strains. Table 3 reports the diameter of the bacterial-free zone around the disk-shaped samples of OCPdAg5 and αTCPdAg5 (8.2 and 4.7 % content of AgNPs).

Table 3 - Antibacterial activity: diameter of the inhibition zone (in millimeter) against ATCC reference strains.

Reference strains	**OCPdAg5**	**αTCPdAg5**	**GMN 10 μg[a]**
S. aureus ATCC 25923	7 ± 1	7 ± 1	20 ± 1
S. epidermidis ATCC 12228	13 ± 1	11 ± 1	25 ± 1
E. faecalis ATCC 29212	6 ± 1	7 ± 1	12 ± 1
E. coli ATCC 25922	12 ± 1	12 ± 1	19 ± 1
K. pneumoniae ATCC 9591	10 ± 1	9 ± 1	18 ± 1
P. aeruginosa ATCC 27853	12 ± 1	12 ± 1	19 ± 1

[a]Disks containing gentamicin 10 μg (Oxoid SpA, Italy) were used as positive controls.
All experiments were performed on duplicate, on different days.

These materials, which were selected as they demonstrated to be effective against bacterial growth without cytotoxicity on osteoblast, were assayed against clinical isolates of *S. epidermidis* and P. *aeruginosa* presenting different antibiotic susceptibilities. In particular, the panel of samples included methicillin-resistant *S.*

epidermidis (MRSE) and MDR *P. aeruginosa*. The antibiotic-resistance profile of each clinical strain and the antibacterial activities of the composite materials are reported in Table 4.

Table 4 - Antibacterial activity: diameter of the inhibition zone (in millimeter) against clinical isolates.

S. epidermidis	**OCPdAg5**	**αTCPdAg5**	**GMN 10 μg**	**IPM 10 μg**	**Antibiotic-resistance profile**
Isolate 1	10 ± 1	8 ± 1	9 ± 1	52 ± 1	CM^S, E^S, LVX^S, OX^S, TE^S, SXT^S
Isolate 2	10 ± 1	7 ± 1	27 ± 1	24 ± 1	CM^S, **E^R**, LVX^S, OX^S, TE^S, SXT^S
Isolate 3[§]	10 ± 1	8 ± 1	NA*	37 ± 1	CM^S, **E^R**, **GMN^R**, **LVX^R**, **OX^R**, TE^S, SXT^S
Isolate 4[§]	10 ± 1	7 ± 1	NA*	28 ± 1	CM^S, **E^R**, **GMN^R**, **LVX^I**, **OX^R**, TE^S, **SXT^I**
Isolate 5[§]	10 ± 1	8 ± 1	25 ± 1	12 ± 1	CM^S, **E^R**, GMN^S, LVX^S, **OX^R**, TE^S, **SXT^R**
Isolate 6[§]	10 ± 1	8 ± 1	NA*	NA*	**CM^R**, **E^R**, **GMN^R**, **LVX^R**, **OX^R**, TE^S, **SXT^R**
Isolate 7[§]	10 ± 1	8 ± 1	NA*	NA*	**CM^R**, **E^R**, **GMN^R**, **LVX^R**, **OX^R**, TE^S, **SXT^I**
P. aeruginosa					
Isolate 1	8 ± 1	7 ± 1	16 ± 1	25 ± 1	AN^S, FEP^S, CAZ^S, CIP^S, GMN^S, IPM^S, MEM^S, TZP^S
Isolate 2	11 ± 1	9 ± 1	16 ± 1	26 ± 1	AN^S, FEP^S, CAZ^S, CIP^S, GMN^S, IPM^S, MEM^S, TZP^S
Isolate 3	10 ± 1	9 ± 1	17 ± 1	25 ± 1	AN^S, FEP^S, CAZ^S, CIP^S, GMN^S, IPM^S, MEM^S, TZP^S
Isolate 4[#]	10 ± 1	7 ± 1	NA*	11 ± 1	AN^S, **FEP^R**, **CAZ^R**, **CIP^R**, **GMN^R**, **IPM^R**, **MEM^R**, **TZP^R**, **TGC^R**, CS^S
Isolate 5[#]	9 ± 1	8 ± 1	NA*	11 ± 1	AN^S, FEP^S, **CAZ^R**, **CIP^R**, **GMN^R**, **IPM^R**, **MEM^R**, **TZP^R**, CS^S
Isolate 6[#]	7 ± 1	7 ± 1	NA*	11 ± 1	**AN^R**, **FEP^R**, **CAZ^R**, **CIP^R**, **GMN^R**, **IPM^I**, **MEM^I**, **TZP^R**, CS^S
Isolate 7[#]	11 ± 1	8 ± 1	NA*	NA*	**AN^R**, **FEP^R**, **CAZ^R**, **CIP^R**, **GMN^R**, **IPM^R**, **MEM^I**, **TZP^R**, CS^S

AN = Amikacin; CM = Clindamicyn; E = Erythromycin; FEP = Cefepime; CAZ = Ceftazidime; CIP = Ciprofloxacin; GMN = Gentamicin; IPM = Imipenem; MEM = Meropenem; TZP = Piparacillin/Tazobactam; TGC = Tigecycline; CS = Colistin; LVX = Levofloxacin; OX = Oxacillin; TE = Tetracycline; SXT = Trimethoprim/Sulfamethoxazole

R = Resistant; S = Susceptible; I = Intermediate, as defined following the EUCAST guidelines

*NA, not appearing; [§]*Staphylococcus* species resistant to oxacillin were declared, by convention, methicillin-resistant.

[#]*Pseudomonas* species defined MDR as resistant to at least three agents from a variety of antibiotic classes.

Both OCPdAg5 and αTCPdAg5 displayed antibacterial properties against all the tested clinical isolates and the comparison of the diameters of the inhibition zone indicates a greater activity of OCPdAg5 in comparison to αTCPdAg5, possibly due to the higher content of AgNPs (8.2 vs. 4.7%). Notably, these selected biomaterials at this AgNPs content did not interfere with osteoblast proliferation and activity indicating a specific antibacterial property. Both samples proved to be effective towards methicillin-sensitive *S. epidermidis* (MSSE) and MRSE strains that were resistant to erythromycin or gentamicin or levofloxacin or trimethoprim/sulfamethoxazole, in addition to oxacillin and all other β-lactam and cephalosporin antibiotics that share structural similarity with methicillin. Of note, tested samples were also active against two isolates that were resistant to the GMN/IPM reference disk controls in the KB diffusion method, and that were susceptible only to tetracycline as determined by EUCAST clinical zone diameter breakpoints. Considering the selected *P. aeruginosa* strains, both OCPdAg5 and αTCPdAg5 showed a remarkable inhibitory property towards both sensitive and heterogeneous MDR phenotypes.

4. Conclusions

The results of this study indicate that polydopamine can be used as a tool to trigger the deposition of silver nanoparticles onto calcium phosphates. The different morphology of OCP and αTCP plays an important role both on polydopamine functionalization and on AgNPs deposition. In fact, PDA forms a homogeneous layer on the surface of the big plate-like OCP crystals and aggregates on the αTCP particles. The different arrangement of PDA could justify the greater amount of AgNPs loaded on polydopamine functionalized OCP compared to αTCP surfaces. Moreover, the two calcium phosphate supports play a key role on osteoblast behavior towards final composite materials: the amount of AgNPs that does not give any cytotoxicity is

significantly greater on functionalized OCP (8.2 wt%) than on functionalized αTCP (4.7 wt%). Up to these AgNPs contents, the developed composite materials provide suitable supports for osteoblast adhesion, proliferation and differentiation, whereas they display a remarkable antibacterial activity towards the main relevant sensitive and multi-drugs resistant bacteria, demonstrating good potentiality for the treatment of bone or prosthetic joint infections.

Acknowledgements.

The authors are grateful to Rizzoli Orthopaedic Institute (funds 5 X 1000 year 2013, cod. 6191) and to the University of Bologna. Authors thank dr. Laura Sicuro for *in vitro* experiment support.

Abbreviations

OCP	Octacalcium phosphate
αTCP	α-tricalcium phosphate
HA	hydroxyapatite
βTCP	β-tricalcium phosphate
CaPs	Calcium phosphates
PDA	Polydopamine
AgNPs	Silver nanoparticles
OCPd	PDA functionalized OCP
αTCPd	PDA functionalized αTCP
OCPdAg	PDA functionalized OCP with deposited AgNPs
αTCPdAg	PDA functionalized αTCP with deposited AgNPs
AFM	Atomic Force Microscopy
SEM	Scanning electron microscopy
XRD	X-ray diffraction
ICP	Inductively coupled plasma mass *spectrometry*
OB	Osteoblast
DMEM	Dulbecco's modified Eagle's medium
WST1	Tetrazolium salt
LDH	Lactate dehydrogenase
NR	Neutral Red
ALP	Alkaline phosphatase
OSTC	Osteocalcin
IL6	Interleukin 6
qPCR	Quantitative Polymerase Chain Reaction
ALPL	Alkaline phosphatase liver/bone/kidney isozyme
CASP3	Caspase 3
BGLAP	Osteocalcin
RUNX2	Runt related transcription factor 2
GAPDH	Glyceraldehyde-3-phosphate dehydrogenase
MALDI-TOF MS	Matrix-assisted laser desoption/ionization time of-flight mass spectrometry
KB	Kirby-Bauer
GMN	Gentamicin
IPM	Imipenem
MRSE	Methicillin-resistant *S. epidermidis*
MSSE	Methicillin-sensitive *S. epidermidis*
MDR	Multi-drug resistant

References

[1] O. Suzuki, Octacalcium phosphate: Osteoconductivity and crystal chemistry, Acta Biomater. 6 (2010) 3379–3387.

[2] O. Suzuki, S. Kamakura, T. Katagiri, M. Nakamura, B. Zhao, Y. Honda, R. Kamijo, Bone formation enhanced by implanted octacalcium phosphate involving conversion into Ca-deficient hydroxyapatite, Biomaterials 27 (2006) 2671-2681.

[3] Y. Honda, T. Anada, S. Kamakura, S. Morimoto, T. Kuriyagawa, O. Suzuki, The effect of microstructure of octacalcium phosphate on the bone regenerative property, Tissue Eng. A 15 (2009) 1965–1973.

[4] K. Kobayashi, T. Anada, T. Handa, N. Kanda, M. Yoshinari, T. Takahashi, O.Suzuki, Osteoconductive property of a mechanical mixture of octacalcium phosphate and amorphous calcium phosphate, ACS Appl. Mater. Interfaces 6 (2014) 22602−22611.

[5] E. Boanini, P. Torricelli, M. Fini, F. Sima, N. Serban, I.N. Mihailescu, A. Bigi, Magnesium and strontium doped octacalcium phosphate thin films by matrix assisted pulsed laser evaporation, J. Inorg. Biochem. 107 (2012) 65–72.

[6] R.J. Dekker, J.D. de Bruijn, M. Stigter, F. Barrere, P. Layrolle, C.A. van Blitterswijk, Bone tissue engineering on amorphous carbonated apatite and crystalline octacalcium phosphate-coated titanium discs, Biomaterials 26 (2005) 5231–5239.

[7] A. Bigi, E. Boanini, M. Borghi, G. Cojazzi, S. Panzavolta, N. Roveri, Synthesis and hydrolysis of octacalcium phosphate: effect of sodium polyacrylate, J. Inorg. Biochem. 75 (1999) 145–151.

[8] A. Bigi, E. Boanini, G. Falini, S. Panzavolta, N. Roveri, Effect of sodium polyacrylate on the hydrolysis of octacalcium phosphate, J. Inorg. Biochem. 78 (2000) 227–233.

[9] M.S. Tung, B. Tomazic, W.E. Brown, The effects of magnesium and fluoride on the hydrolysis of octacalcium phosphate. Arch. Oral Biol. 37 (1992) 585–591.

[10] O. Suzuki, H. Yagishita, M. Yamazaki, T. Aoba, Adsorption of bovine serum albumin onto octacalcium phosphate and its hydrolyzates. Cells Mater. 5 (1995) 45–54.

[11] N. Miyatake, K.N. Kishimoto, T. Anada, H. Imaizumi, E. Itoi, O. Suzuki, Effect of partial hydrolysis of octacalcium phosphate on its osteoconductive characteristics. Biomaterials 30 (2009) 1005–1014.

[12] Y. Shiwaku, T. Anada, H. Yamazaki, Y. Honda, S. Morimoto, K. Sasaki, O. Suzuki. Structural, morphological and surface characteristics of two types of octacalcium phosphate-derived fluoride-containing apatitic calcium phosphates. Acta Biomaterialia 8 (2012) 4417–4425.

[13] E. Boanini, S. Panzavolta, K. Rubini, M. Gandolfi, A. Bigi,Effect of strontium and gelatin on the reactivity of a-tricalcium phosphate. Acta Biomater. 6 (2010) 936–942.

[14] M. Frasnelli, V.M. Sglavo, Effect of Mg2+ doping on beta–alpha phase transition in tricalcium phosphate (TCP) bioceramics, Acta Biomater. 33 (2016) 283–289.

[15] A. Bigi, S. Panzavolta, K. Rubini, Setting mechanism of a biomimetic bone cement, Chem. Mater. 16 (2004) 3740-3745.

[16] M. Bohner, A.K. Malsy, C.L. Camire´, U. Gbureck, Combining particle size distribution and isothermal calorimetry data to determine the reaction kinetics of a-tricalcium phosphate–water mixtures, Acta Biomater. 2 (2006) 343–348.

[17] K. Chaloupka, Y. Malam, A.M. Seifalian, Nanosilver as a new generation of nanoproduct in biomedical applications, Trends Biotechnol. 28 (2010) 580–588.

[18] E. Boanini, P. Torricelli, M.C. Cassani, G.A. Gentilomi, B. Ballarin, K. Rubini, F. Bonvicini, A. Bigi, Cationic-anionic polyelectrolyte interaction as a tool to graft silver nanoparticles on hydroxyapatite crystals and prevent cytotoxicity, RSC Adv. 4 (2014) 645-652.

[19] H. Lee, S.M. Dellatore, W.M. Miller, P.B. Messersmith, Mussel-inspired surface chemistry for multifunctional coatings, Science 318 (2007) 426-430.

[20] Y. Liu, K. Ai, L. Lu, Polydopamine and its derivative materials: synthesis and promising applications in energy, environmental, and biomedical fields. Chem. Rev. 114 (2014) 5057−5115.

[21] V. Ball, I. Nguyen, M. Haupt, C. Oehr, C. Arnoult, V. Toniazzo, D. Ruch, The reduction of Ag+ in metallic silver on pseudomelanin films allows for antibacterial activity but does not imply unpaired electrons, J. Colloid Interface Sci. 364 (2011) 359–365.

[22] E. Boanini, M. Gazzano, K. Rubini, A. Bigi, Collapsed octacalcium phosphate stabilized by ionic substitutions, Cryst. Growth Des. 10 (2010) 3612–3617.

[23] A. Bigi, E. Boanini, R. Botter, S. Panzavolta, K. Rubini, α-Tricalcium phosphate hydrolysis to octacalcium phosphate: effect of sodium polyacrylate, Biomaterials 23 (2002) 1849–1854.

[24] A. Croxatto, G. Prod'hom, G. Greub, Applications of MALDI-TOF mass spectrometry in clinical diagnostic microbiology, FEMS Microbiol. Rev. 36 (2012) 380-407.

[25] EUCAST: The European Committee on Antimicrobial Susceptibility Testing. Breakpoint tables for interpretation of MICs and zone diameters. Version 6.0, 2016. http://www.eucast.org.

[26] Clinical and Laboratory Standards Institute. Performance Standards for Antimicrobial Susceptibility Testing; Twenty-fifth Informational Supplement. CLSI document M100-S25 (2015)

[27] E. Ko, K. Yang, J. Shin, S.-W. Cho, Polydopamine-assisted osteoinductive peptide immobilization of polymer scaffolds for enhanced bone regeneration by human adipose-derived stem cells, Biomacromolecules 14 (2013) 3202−3213.

[28] T.S. Sileika, H.D. Kim, P. Maniak, P.B. Messersmith, Antibacterial performance of polydopamine-modified polymer surfaces containing passive and active components, ACS Appl. Mater. Interfaces 3 (2011) 4602–4610.

[29] UNI EN ISO 10993-5- Biological evaluation of medical devices Part 5: Tests for in vitro cytotoxicity. 2009

[30] A. Degterev, M. Boyce, J. Yuan, A decade of caspases. Oncogene 22 (2003) 8543-8567.

[31] R. Olivares-Navarrete, S.L. Hyzy, P.J. Slosar, J.M. Schneider, Z. Schwartz, B.D. Boyan, Implant materials generate different peri-implant inflammatory factors: poly-ether-ether-ketone promotes fibrosis and microtextured titanium promotes osteogenic factors, Spine 40 (2015) 399-404.

[32] S. Morimoto, T. Anada, Y. Honda, O. Suzuki, Comparative study on in vitro biocompatibility of synthetic octacalcium phosphate and calcium phosphate ceramics used clinically, Biomed Mater. 7 (2012) 045020. doi: 10.1088/1748-6041/7/4/045020.

[33] M. Kamitakahara, C. Ohtsuki, T. Miyazaki, Review paper: behavior of ceramic biomaterials derived from tricalcium phosphate in physiological condition, J. Biomater. Appl. 23 (2008) 197-212.

[34] E. Boanini, P. Torricelli, M. Gazzano, M. Fini, A. Bigi, Crystalline calcium alendronate obtained by octacalcium phosphate digestion: A new chance for local treatment of bone loss diseases? Adv. Mater. 25 (2013) 4605-4611.

[35] E. Boanini, P. Torricelli, L. Forte, S. Pagani, N. Mihailescu, C. Ristoscu, I. N. Mihailescu, A. Bigi, Antiresorption implant coatings based on calcium alendronate and octacalcium phosphate deposited by matrix assisted pulsed laser evaporation, Colloid Surf. B-Biointerfaces 136 (2015) 449-456.

[36] U. Mayr-Wohlfart, J. Fiedler, K.P. Gùnter, W. Puhl, S. Kessler, Proliferation and differentiation rates of a human osteoblast-like cell line (SaOS-2) in contact with different bone substitute materials, J. Biomed. Mater. Res. 57 (2001) 132-139.

[37] A. Ehara, K. Ogata, S. Imazato, S. Ebisu, T. Nakano, Y. Umakoshi, Effects of alpha-TCP and TetCP on MC3T3MC3T3TetCP on MC3T3 proliferation, differentiation and mineralization, Biomaterials 24 (2003) 831-836.

[38] M.B. Greenblatt, J.N. Tsai, M.N. Wein, Bone turnover markers in the diagnosis and monitoring of metabolic bone disease. Clin. Chem. 63 (2017) 464-474.

[39] M. Shahi, A. Peymani, M. Sahmani, Regulation of bone metabolism, Rep. Biochem. Mol. Biol. 5 (2017) 73-82.

Graphical Abstract

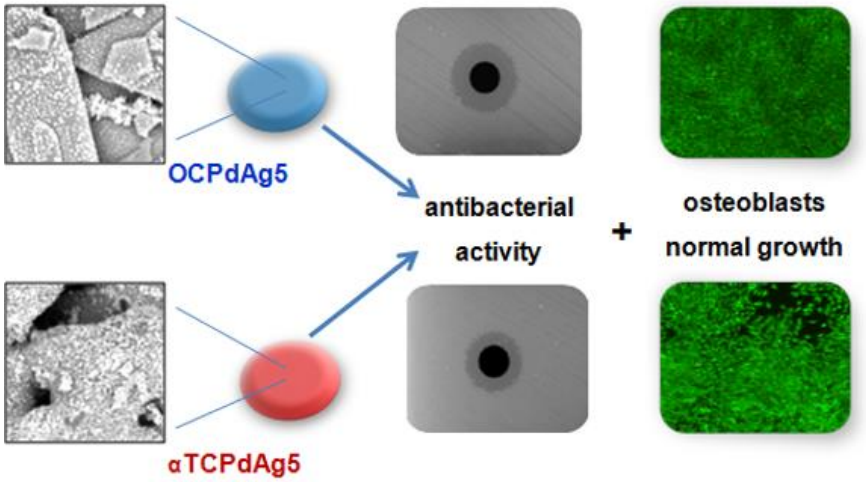

Synopsis

Polydopamine mediated deposition of silver nanoparticles on calcium phosphates provides composite materials, which support osteoblast growth and differentiation, whereas they inhibit the growth of multi-drug resistant Gram positive and Gram negative bacteria.

Highlights

- Polydopamine functionalized calcium phosphates trigger AgNPs deposition
- Octacalcium phosphate and αTCP materials at different AgNPs content are proposed
- Composite materials are able to inhibit antibiotic-resistant clinical isolates
- These antibacterial materials also support osteoblast viability and differentiation